This is a repository copy of *Geodynamics of very high speed transport systems*.

White Rose Research Online URL for this paper:
http://eprints.whiterose.ac.uk/154317/

Version: Accepted Version

Article:

Geodynamics of very high speed transport systems

Authors: D.P. Connolly[1][*] and P. Alves Costa[2]

[1] Institute for High Speed Rail and Systems Integration, Civil Engineering, University of Leeds, UK. d.connolly@leeds.ac.uk

[2] Faculty of Engineering, University of Porto, Portugal. pacosta@fe.up.pt

[*] Corresponding author

Abstract

This work reveals the existence of a new dynamic load amplification mechanism due to ground surface loads. It is caused by the interaction between a moving vehicle's axle configuration and the vibration characteristics of the underlying soil-guideway system. It is more dominant than the traditionally considered 'critical velocity' dynamic amplification mechanism of the guideway-ground structure, and is of relevance to very high speed transport systems such as high speed rail.

To demonstrate the new amplification mechanism, first a numerical model is developed, capable of simulating ground-wave propagation in the presence of a series of discrete high speed loads moving on a soil-guideway system. The model couples analytical equations for the transportation system guideway with the thin-layer element method for ground simulation. As a practical example, it is validated using high speed railroad field data and then used to analyse the response of a generalised single moving load at high speed. Next the effect of multiple discrete vehicle-guideway contact points is studied and it is shown that dynamic amplification is highly sensitive to load spacing when the speed is greater than the critical velocity. In particular, large resonant effects occur when the axle/magnet loading frequency and the propagating wave vibration frequency of the soil-guideway structure are equivalent. As an example, it is shown that for an individual case, although critical velocity might increase displacements by 50-100%, for the same scenario, axle configuration can increase displacements by 400%. It is also shown that resonance is sensitive to the total number of loading points and the individual frequencies excited by various spacings. The findings are important for current (e.g. high speed railway) and potential future (e.g. hyperloop) transport systems required to operate at speeds either close-to, or greater than the critical velocity of their supporting guideway-soil structure. In such situations, it is important to design the vehicle and supporting structure(s) as a combined system, rather than in isolation.

1. Introduction

The aspirational speeds of vacuum transport and car technology are 1200 km/h [1] and 1600 km/h [2] respectively. Also, the current railway speed record is 603km/h and 574km/h for Maglev and steel-wheel technologies respectively. These indicate the desire to increase the operational speed of transport systems. To achieve these high speeds under commercial operating conditions requires a high performance guideway that safely shepherds the vehicle in the desired direction. In practise, steel-wheel/maglev trains are guided by concrete/ballast railway track, automobiles move upon flexible/rigid pavement, and hyperloop systems will operate inside tubes ([3]).

Some sections of road and railway guideways are elevated above the natural ground using viaducts to avoid challenging ground conditions. However, as vehicle speeds increase, vertical and horizontal guideway alignment tolerances also reduce, meaning the radius of vertical/horizontal curves must be much greater. Considering very high speed technologies are only practical over large distances, a guideway with very straight alignment is then likely to encounter significant changes in topography and ground conditions along its route. Thus, considering the cost of very deep cuttings (e.g. through hills/mountains), it is unlikely that an entire route can be supported on viaduct. This means that for many practical applications, even if viaducts are the de-facto guideway support, sections of the route will likely be constructed underground ([4]) or close to the earth's surface.

If the guideway of a transport system is supported directly by earthworks ([5], [6]), then the moving load has the potential to approach or exceed the 'critical velocity' of its supporting guideway-soil system ([7], [8], [9]). In this situation, significant displacement amplification of the guideway occurs, which can be safety-critical at high speed. Dynamic amplification is a well-accepted design consideration when constructing transportation infrastructure, particularly in the field of high speed rail.

To de-risk railways from critical velocity induced deflection amplification, traditional designers use highly engineered granular soils ([10]) and modern compaction methods to maximise foundation stiffness. However, as vehicle speeds continue to increase, artificial soil stiffening (e.g. lime or cement) is sometimes required to further increase shear wave velocities (e.g. [11]). This is expensive and thus challenging to justify over larger distances (e.g. across significant length of a transport network), particularly if very high soil shear wave velocities are needed. Therefore it may be necessary to run at speeds close to, or above the critical velocity.

To investigate this challenge, this paper uses numerical analysis to assess the effect of loads moving at different ratios of the critical speed. In particular, multi-load combinations are investigated and the relationship between axle spacing and support vibration frequency are studied. This is important because the ground and guideway both have vibration frequencies (Figure 1b-c) which combine to yield a common vibration frequency for the entire system. The vehicle also has excitation frequencies associated with its axle/magnet spacing (Figure 1a - hereafter called 'axles'), at a certain speed. If the vehicle excitation frequency and the propagating wave vibration frequency of the soil-guideway coincide then there is a potential for resonance.

Although there is a lack of research into moving load resonance relationships, early analytical studies into critical velocity included [12], [13] and [14] who simulated the problem as a generalised point load moving on an elastic foundation. Krylov [15] expended upon this and used Green's functions to better tailor the analysis towards high speed rail problems. This was followed using similar approaches proposed by [16] and [17]. Alternatively, [18] proposed a semi-analytical approach, where a more complex track model was coupled with a Thomson-Haskell method for the soil.

As an alternative to analytical critical velocity modelling [19], [20], [21] developed 2D finite element models. To overcome the limitations of 2D modelling, 3D approaches were proposed by [22], [23], [24], [25], [26], [27], [28]. A challenge with 3D approaches however is that they require significant computational effort to solve. Therefore 2.5D models were also proposed by [29], [30], [31], [32]. Additionally, a variety of these modelling strategies were combined to make wide ranging findings into critical velocity effects ([9]).

Despite the large number of studies into transport ground dynamics, most have focused on either the effect of multiple axles at speeds lower than the critical speed, or the effect of a single axle above the critical speed. Therefore this paper investigates the effect of multiple axles moving at speeds close to or greater than the critical velocity. First a high-accuracy, yet computationally efficient modelling approach is presented based upon the thin-layer element method. Then a generic high speed rail case is discussed. First the case of a single axle is presented, followed by a multi-axle case. It is shown that when approaching the critical speed (e.g. >90%), resonance becomes a governing parameter on vibration amplification. In particular, resonance can have a larger amplification effect compared to the amplification induced by moving load speed.
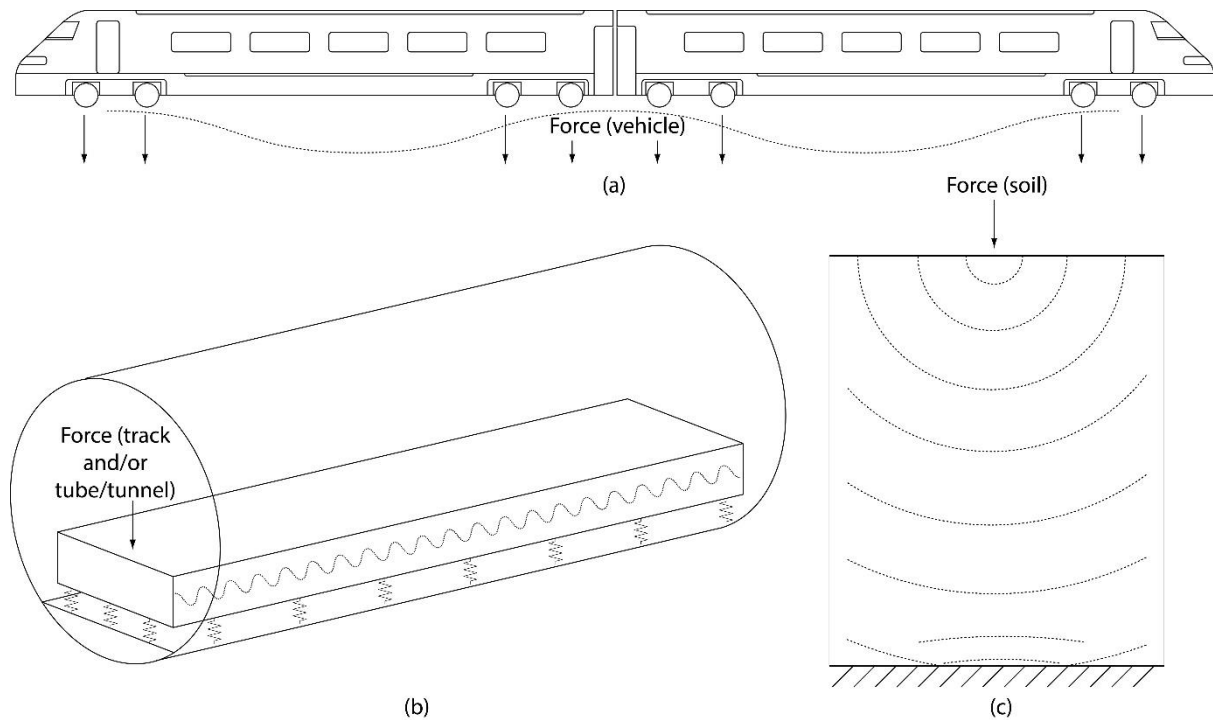
Figure 1: Vibration of linear transport infrastructure, (a) Vehicle axles, (b) Track and/or tube/tunnel structure, (c) Soil. Dashed black lines indicate examples of wave propagation.

2. Numerical model description

The numerical model is comprised of two coupled sub-models, 1) an analytical guideway model, and 2) a thin-layer element ground model. The frequency-wavenumber domain is used to solve both sub-models and coupling is performed in the same domain. This approach is advantageous because the thin-layer method allows for deep soil wave propagation to be simulated quickly even at large depths. This is vital for moving load simulations close-to and above the critical velocity. Further, the analytical guideway model allows for guideway displacements to be computed in a rapid and straightforward manner.

2.1 Soil

The thin-layer element method (TLM) is used to compute the 3D response of the soil. It is advantageous because it can efficiently simulate arbitrarily layered soils (i.e. it has no limitations regarding low-stiffness sandwich layers, or layer thicknesses). It assumes that the soil behaviour is linear elastic, and non-linear ([33], [34], [35]) behaviour is ignored.

First the soil domain is discretised into a finite number (n) of horizontal layers which must be parallel and thin with respect to all wavelengths under consideration. In the vertical direction,

displacements are computed assuming numerical approximation of the solution through parabolic shape functions. This assumption is valid as long as all thin layers thicknesses' (h) fulfil the criteria:

$$h = \frac{wavelength}{8} = \frac{2\pi}{8k_{max}}$$ (1)

where k_{max} is the maximum wavenumber. Three-node quadratic elements are used to accurately simulate stress-strain behaviour, resulting in a total of 17 nodes per wavelength. k_x and k_y are wavenmbers in the x and y directions respectively. The lower boundary can be modelled as a half-space, however for the purpose of this work, to create a well-defined soil natural frequency, the majority of cases consider it to be rigid bedrock. Although such a shallow bedrock might be rare in real-life, it presents a useful test case to accentuate the analysis and discussion.

The problem is solved in the frequency-wavenumber domain by computing the response of individual frequencies under steady-state harmonic conditions. This is achieved via:

$$(\mathbf{K} - \omega^2\mathbf{M})\mathbf{U} = \mathbf{P}$$ (2)

where **P** is traction, **U** is displacement, **M** is the mass matrix and ω is frequency. Further, **K** is the stiffness matrix ~~shown in Equation 3~~:

$$\mathbf{K} = \mathbf{K_0} + ik_x\mathbf{K_1} + ik_y\mathbf{K_2} + k_x^2\mathbf{K_3} + k_y^2\mathbf{K_4} + k_xk_y\mathbf{K_5}$$ (3)

where $i = \sqrt{-1}$ and **K**[0-5] are given in [11]. Finally, frequency independent hysteric damping is simulated using complex functions for Lames elastic constants: $\lambda = \lambda(1 + 2i\xi_\lambda)$ and $\mu = \mu(1 + 2i\xi_\mu)$, where ξ_λ is the damping ratio for dilatational waves and ξ_μ is the damping ratio for shear waves. $\xi_\lambda = \xi_\mu$ is assumed in this work.
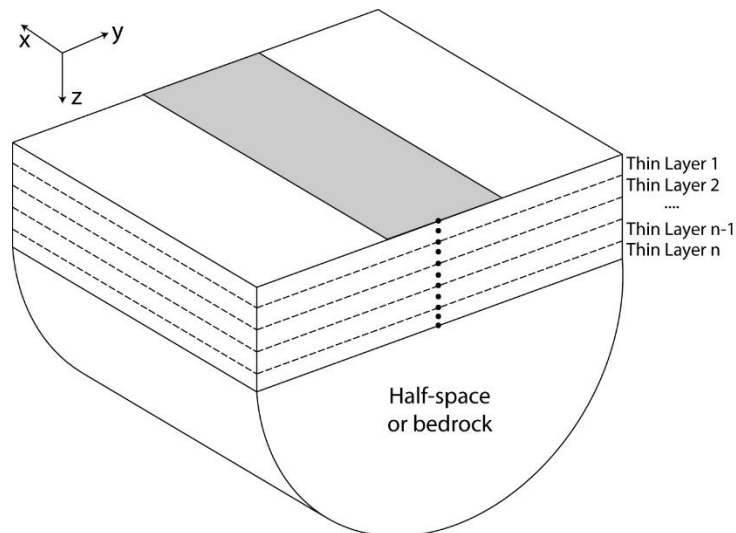
Figure 2 – Soil model discretisation using thin-layer elements

$$\begin{bmatrix} EI_r k_x^4 + k_p^* - \omega^2 m_r & -k_p^* & 0 \\[2ex] -k_p^* & k_p^* + \dfrac{2\omega E_b^* b\alpha}{\tan\left(\dfrac{\omega h_b}{C_p}\right) C_p} - \omega^2 m_s & \dfrac{-2\omega E_b^* b\alpha}{\sin\left(\dfrac{\omega h_b}{C_p}\right) C_p} \\[4ex] 0 & \dfrac{-2\omega E_b^* b\alpha}{\sin\left(\dfrac{\omega h_b}{C_p}\right) C_p} & \dfrac{2\omega E_b^* b\alpha}{\tan\left(\dfrac{\omega h_b}{C_p}\right) C_p} + k_{eq} \end{bmatrix} \begin{Bmatrix} \tilde{u}_r(k_x,\omega) \\ \tilde{u}_s(k_x,\omega) \\ \tilde{u}_{bb}(k_x,\omega) \end{Bmatrix} \qquad (4)$$

$$= \begin{Bmatrix} \tilde{P}(k_x,\omega) \\ 0 \\ 0 \end{Bmatrix}$$

2.2 Guideway model

The guideway model is formulated in the wavenumber-frequency domain as described in [36] and [37]. It is based upon a high speed railway guideway as shown in Figure 3. It comprises rail, railpad, sleeper, and ballast components. Equation 4 describes the equations of motion, where k_x is the Fourier image of x and , m_r and m_s are the mass of rail and sleepers (distributed per metre) respectively. k_p^* is the complex stiffness of the railpad, defined as $k_p^* = k_p(1 + i\omega c_p)$, where c_p is the railpad damping. C_p, E_b and h_b are the compressional wave speed, the Young's modulus and height of the ballast respectively. Finally, b is the contact width between soil and guideway, $\tilde{u}_r$, $\tilde{u}_s$ and $\tilde{u}_{bb}$ are the rail, sleeper, and ballast deflections respectively, and P is force applied by the moving axle load on the upper rail surface.
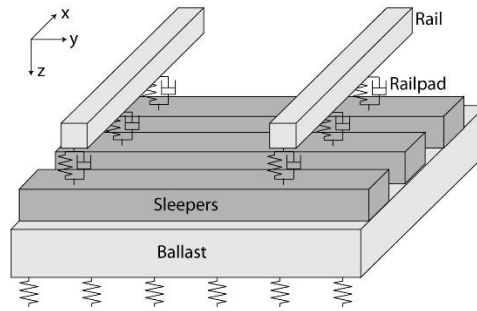
Figure 3 – Railway guideway structure layout

Guideway-subgrade coupling is implemented using a complex stiffness ($\tilde{k}_{eq}(k_x,\omega)$) shown as a spring in Figure 3:

$$\tilde{k}_{eq}(k_x,\omega) = \frac{2\pi}{\int_{-\infty}^{+\infty} \tilde{u}_{zz}^G(k_x,k_y,z=0,\omega) C_{tg} dk_y} \qquad (5)$$

Where $\tilde{u}_{zz}^G$ is the Green's function of the vertical soil surface displacement, extracted from U in equation 2.

As vehicle speed increases and nears critical velocity, there is increased deep-wave propagation inside the soil and across the guideway-ground interface. Therefore coupling is implemented through the equilibrium of forces and the compatibility of displacements across the guideway-soil interface, at the track centre point, assuming relaxed boundary conditions [38]. This is achieved via:

$$C_{tg} = \sin(k_y b)/k_y b$$

After the TLM is used to compute, $\tilde{k}_{eq}(k_x, \omega)$, it is inserted into the guideway model (Equation 4), thus yielding the displacements of its individual components. These displacements are then scaled linearly depending upon the moving load magnitude. The rail response, $\tilde{u}_r(k_x, \omega)$, is used throughout this work as the measure of guideway deflection.

The displacement Green's function, $u^g(k_x, k_y, \omega)$, relates the input force and displacement response of the system. The displacement Green's function scaled by a load of arbitrary magnitude is denoted, $G_u(k_x, k_y, \omega)$, and obtained via:

$$G_u(k_x, k_y, \omega) = (L(k_x, \omega)C_{tg})u^g(k_x, k_y, \omega) \tag{6}$$

Where, $L(k_x, \omega)C_{tg}$ is a function that scales the load transmitted from guideway to ground using the equivalent stiffness and lower track displacement [11]. Finally, the ground displacement response in the frequency-wavenumber domain is converted to the time-space domain using:

$$R(x, y, t) = \frac{1}{(2\pi)^3} \int_{-\infty}^{\infty} \int_{-\infty}^{\infty} \int_{-\infty}^{\infty} R(k_x, k_y, \omega) \, e^{i(\omega t - k_x x - k_y y)} dk_x dk_y d\omega \tag{7}$$

It should also be noted that the moving load effect is accounted for by using the shift property of the Fourier transform, relating frequency and wavenumber domains. This is achieved via: $\omega = \Omega - k_x V_t$, where V_t is train speed and Ω is excitation frequency, which is set to 0Hz.

2.3 Validation

When a moving load approaches the critical speed of its soil-guideway structure, dynamic guideway amplification occurs. This is governed by wave propagation in the support-guideway system, which any prediction model must be able to simulate accurately. Therefore Figure 4 shows a comparison between the proposed TLM results and field data collected during the passage of a high speed train on a ballasted line in Sweden (critical velocity ≈215km/h). The details of the vehicle, guideway and soil properties are given in [39]. Results are presented for 2 speeds, both of which show much higher guideway deflections (10-15mm) than the typically allowable ≈1-2mm on high speed railway lines. The proposed model predicts the displacement response with high accuracy in both cases, with strong correlation in shape and magnitude. The small discrepancies are likely to be due to inaccuracies in input data, stemming from measurement accuracy and uncertainties associated with spatial variations in soil properties.
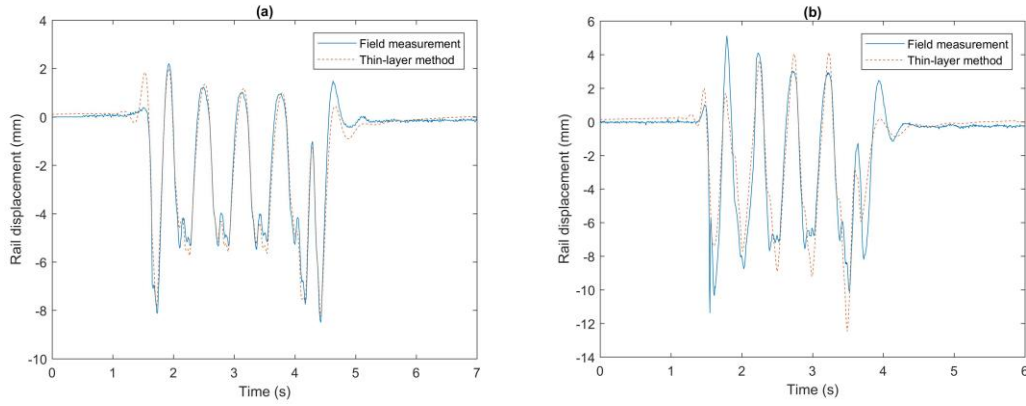
Figure 4 – Displacement time history validation, a) 140 km/h, b) 180km/h

3. Methodology

The analytical-TLM model is used to investigate dynamic guideway amplification due to the relationship between axle spacing and propagating wave vibration frequency of the combined guideway-ground system. Although a variety of current/future transport modes might operate at speeds comparable or greater than the critical velocity, guideway systems are likely to be refined to achieve these high speeds. Therefore, rather than attempt to anticipate future guideway designs, analysis is undertaken using the simplified railway-type guideway described earlier. However, as a variety of bending stiffness' are tested to give insights into how alternative systems might behave.

$$F_s = \frac{V_s}{4H} \tag{8}$$

3.1 Analysis parameters

Four soil configurations are investigated, three with shallow bedrock and a fourth which is a half-space (Table 1). Shallow bedrock is chosen for three cases because due to the lower boundary condition, the first ground natural frequency is highly prominent. This frequency is defined by Equation 8 ([40]), where Vs is the shear wave speed, H is layer thickness and F_s is the first ground natural frequency. This makes it straightforward to make comparisons between infrastructure frequencies and vehicle axle spacing, however the analysis is still valid for other soil stratum configurations. Note though that the infinitely deep homogeneous soil case does not have a natural frequency, because as H approaches infinity, F_s reduces to zero.

Case	Young's modulus (MPa)	Poisson's ratio	Density (kg/m³)	Shear wave velocity (m/s)	Damping ratio	Bedrock depth (m)	Natural frequency (Hz)
1	50	0.35	2000	96.2	0.03	2	12.03
2	100	0.35	2000	136.1	0.03	2	17.01
3	150	0.35	2000	166.7	0.03	2	20.83
4	50	0.35	2000	96.2	0.03	inf	n/a

Table 1 – Soil properties

Rail	Ei_{r1} (Nm²)	9.17×10^6
	Ei_{r2} (Nm²)	1.29×10^7

	Ei_{r3} (Nm^2)		1.53×10^7
	m_r (kg/m)		120
Railpad	k_p (N/m^2)		5×10^8
	c_p (Ns/m^2)		2.5×10^5
Sleepers	m_s (kg/m)		490
Ballast	h (m)		0.35
	E (MPa)		125
	2b (m)		2.5
	ρ (kg/m^3)		1590

Table 2 – Guideway properties

The previously considered ballasted guideway structure is investigated with the properties shown in Table 2. Three different cases are studied with varying rail bending stiffness, however the rail mass and all guideway components below the rail are kept constant. This allows for analysis into the effect of infrastructure stiffness on system vibration frequency and dynamic amplification, and is important because future transport guideways may have different stiffness's compared to current high speed rail lines. Note that the rail properties in Table 2 are for 2 rails. This combination of four soils and three guideways results in 12 possible critical velocity permutations. The critical velocity is defined as the speed of a point load that gives maximum downward vertical displacement of the guideway rail. This condition can be shown to occur at the load speed at which there is a match between the wavelengths propagating in the guideway and ground.

Guideway stiffness			Soil case		
			1 (50MPa)	2 (100MPa)	3 (150MPa)
1	Soft	Speed (m/s)	112.2	142.8	169.2
		Frequency (Hz)	25.5	38.2	37.7
2	Moderate	Speed (m/s)	118.4	150.0	175.5
		Frequency (Hz)	24.8	37.1	46.5
3	Stiff	Speed (m/s)	122.3	153.1	179.6
		Frequency (Hz)	23.0	36.5	45.6

Table 3 – Critical velocities and frequencies

Regarding the vehicle, it is modelled as a series of point loads, with each axle exerting a force of 180kN. For each test case the speed is varied using ratios of the critical velocity (V_{CV}) of the underlying guideway-ground structures. These are shown in Table 3 and are determined by computing the speed-deflection curve for each case. Note that the critical velocity of soil case 4, regardless of guideway type, is 90m/s. Similarly, axle ~~spacing~~ passage frequency is also varied ~~using as a~~ ratio~~s~~ of critical velocity frequency (F_{CV}). In addition, a lower minimum practical axle spacing limit is set as 2.5m to remove all results caused by an unrealistic superposition of deflections.

4. Numerical analysis

4.1 Single load passage case

Figure 5 shows a comparison between the displacement response of a single load moving on guideway type 2, resting on both homogenous vs layered soils (soils 1 and 4). The homogenous soil shows greater deflection as expected because it has lower stiffness, due its lack of rigid support. The faster vehicle speed gives rise to higher displacements, for both the case of the homogenous and layered ground. This result is alternatively plotted as a 3D soil surface contour in Figure 7. The same observations still hold, however it is clearer to see that the homogenous soil causes a wider area of soil across the 3D surface to experience deflection.

When the load is moving at the critical velocity, the bedrock supported soil shows perturbations after the load has passed (Figure 5b). These are not present for the half-space at the equivalent speed, or for either the half-space or layered ground at the lower speed. This occurs post critical velocity because at this frequency the waves propagating within both the guideway and soil do not impede each other. This is more clearly explained via Figure 6b where the first mode of the soil dispersion curve coincides with the guideway dispersion curve at 25Hz (assuming a rigid base). The ability of waves to propagate at a fixed frequency is confirmed through analysis of the layered ground in Figure 5b, where the frequency of vibration is identical (25Hz). In contrast, Figure 6a shows that the soil is non-dispersive and thus waves cannot propagate at a fixed frequency.

At all speeds greater than the critical velocity, waves propagate, while below it, they cannot. This is only true for ground with dispersive properties and does not occur for homogenous half-spaces because they do not have a propagating wave vibration frequency. However, in practise, true homogenous half-spaces rarely exist.
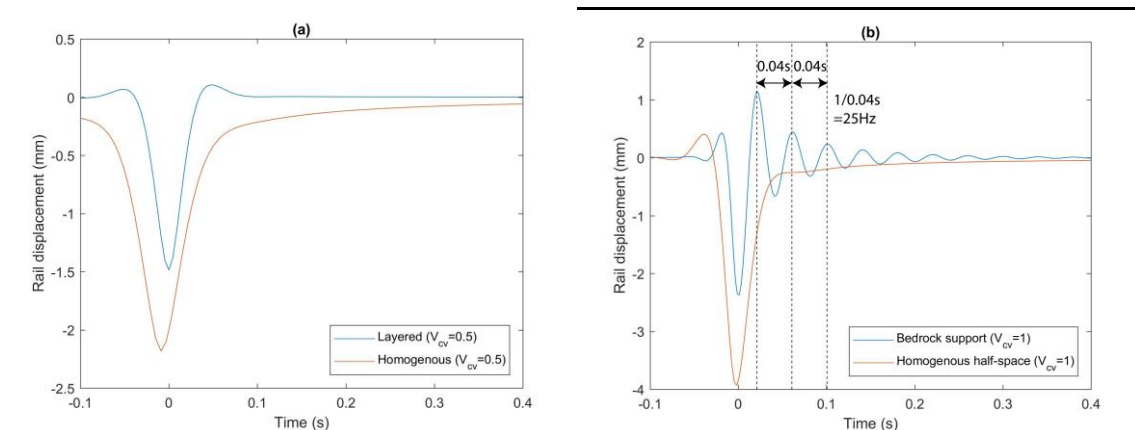
Figure 5 – Time history response due to a moving point load, a) at 50% of critical velocity, b) at 100% of critical velocity
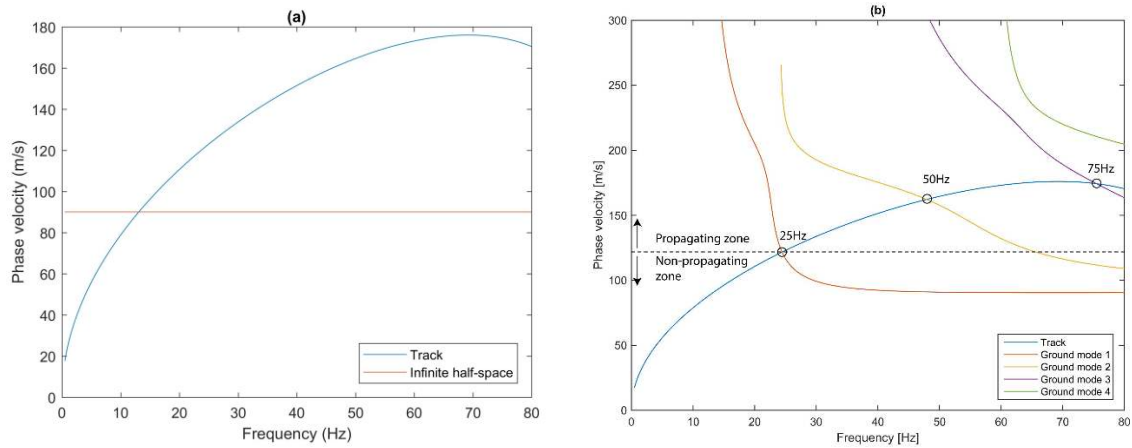
Figure 6 – Dispersion curves, a) Homogenous ground, b) Bedrock (soil case 1)
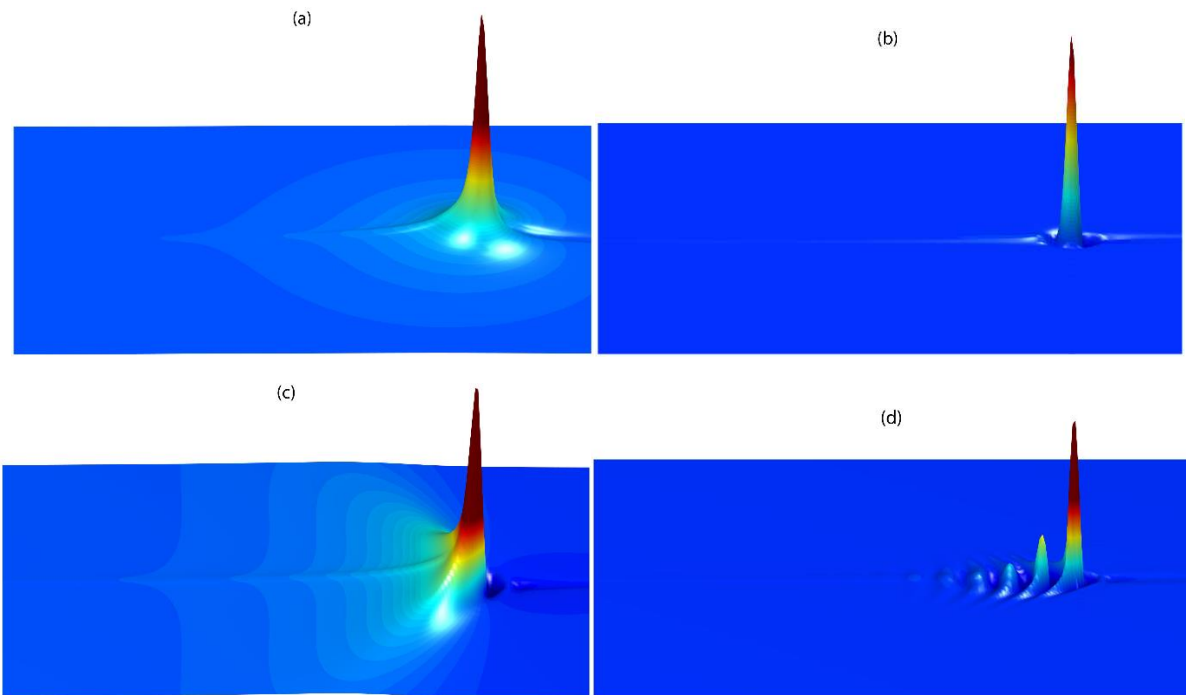
Figure 7 – Normalised ground displacement contours with downward displacements shown as upward deflection, a) homogenous soil with V_{CV}=0.5, b) 2m bedrock soil with V_{CV}=0.5,c) homogenous soil with V_{CV}=1,d) 2m bedrock soil with V_{CV}=1)

Also, Figure 8a shows the frequency spectrum of the response at critical velocity for different bedrock depths. The soil and guideway properties are taken from soil 1-guideway 2, however the bedrock depth is varied between 2-22m. The homogeneous halfspace corresponds to the soil 4-guideway 2 case. It is seen that when bedrock exists a distinct propagating wave vibration frequency is present, however it converges to 0Hz as depth increases. This is consistent with Figure 5 and occurs because a homogenous soil does not have a propagating wave vibration frequency. Figure 8b also shows the relationship between the guideway-ground free-vibration frequency and critical velocity for the bedrock cases. It is seen that there is a positive correlation between both, and that

the free vibration frequency is always between 2-3 times greater than the ~~free vibration~~soil natural frequency. This is expected, and caused by the high relative stiffness of the guideway and the doppler effect.
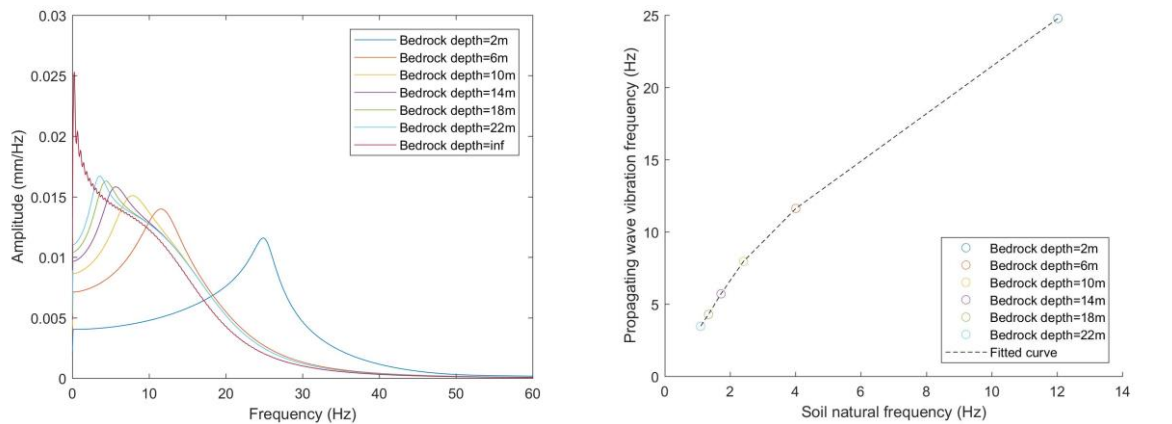
Figure 8 –a) The effect of bedrock on frequency spectrum, b) The relationship between soil natural and propagating wave vibration frequencies

With the aim of investigating post-critical speed behaviour, Figure 9a shows the rail displacement time histories for a single load passage, for a wider range of vehicle speeds. It is seen that post-excitation oscillations only occur when V_{CV}=1, while at speeds below this the response is relatively uniform. Figure 9b shows the corresponding frequency contents of the deflection time histories. At speeds of V_{CV}<1, propagating wave vibration is absent, while at speed V_{CV}=1, there is a distinct peak in the spectra. This is related to the trailing vibrations present in the time history response, which have high amplitudes.

Figure 9b also shows the relationship between the soil natural frequency and the soil-guideway propagating wave vibration frequencies, including at the critical velocity. When V_{CV}=1, the propagating wave vibration frequency is 24.8Hz (Table 3), however higher V_{CV} ratios result in lower propagating wave vibration frequencies, that are closer to the soil natural frequency. This is shown more clearly in Figure 10 where the resonant frequency is plotted against varying vehicle speed. The peak of the spectra is at V_{CV}=1 and decreases with increasing V_{CV}. However, this decrease is relatively minor showing that it may be possible to approximate the critical frequency range of a post critical velocity load, using only the response of a single point-load.

Figure 11 shows the effect of soil stiffness and guideway bending stiffness on resonance. In general it is seen that changing the soil stiffness has a greater impact on frequency response compared to changing guideway stiffness. However, it is also seen that:

1. When below the critical speed, changing soil stiffness shifts the low frequency response (i.e. static stiffness) but doesn't greatly effect high frequency response
2. When above the critical speed, changing soil stiffness has a large effect on resonant frequency and stiffness across the entire frequency range
3. When below the critical speed, changing guideway stiffness has only a small effect on frequency response

4. When above the critical speed, changing guideway stiffness shifts the resonant frequency to a lower value, but the impact is relatively low
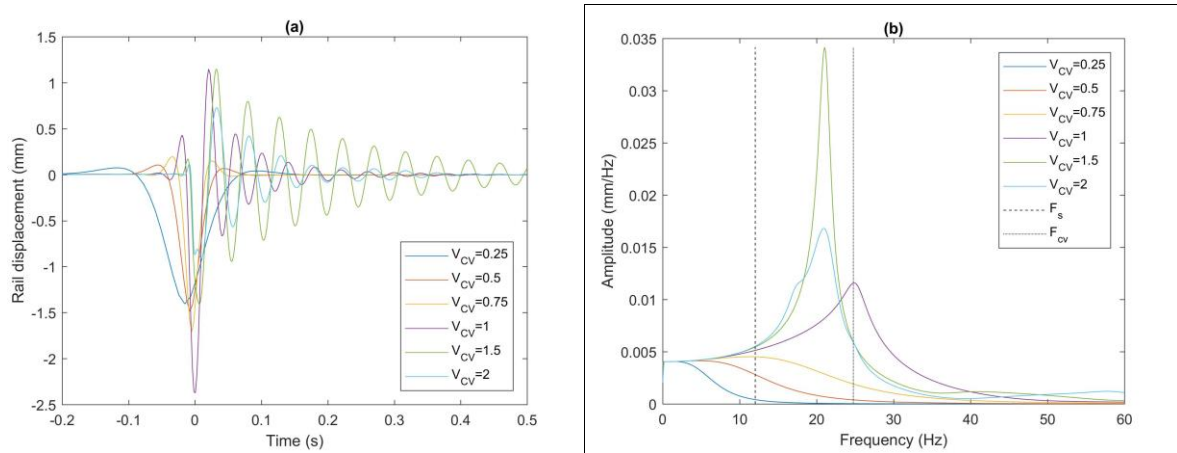
Figure 9 – Single axle response at different ratios of critical velocity, a) Time histories, b) Frequency contents
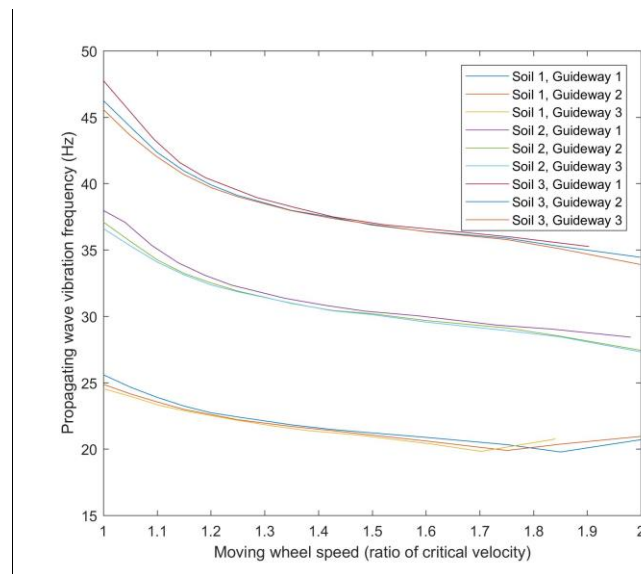
Figure 10 – The effect of axle speed on guideway-ground propagation wave vibration frequency
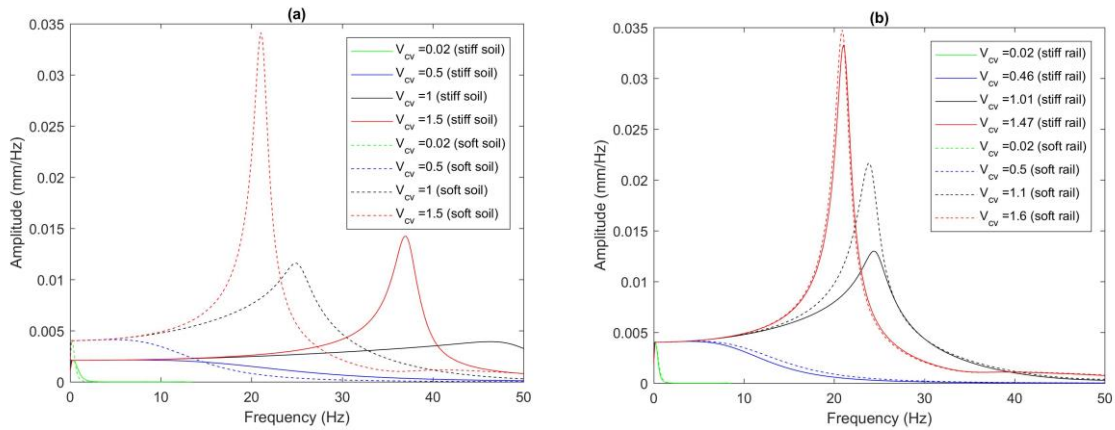
Figure 11 - Single axle response at different ratios of critical velocity, a) Effect of soil stiffness, b) Effect of rail stiffness

4.2 Multi-load passage case

The previous section discusses frequency and critical speed relationships for a single moving load. This is useful to understand the generalised behaviour of the guideway-ground system, however in reality it is likely that current/future transport vehicles will interact with their guideway at multiple discrete loading locations (e.g. multiple axles). Therefore this section expands upon the single moving load analysis to investigate multi-load combinations.

Considering a typical high speed train as a benchmark, it is typically formed from a series of cars, bogies and axles. A detailed discussion regarding rolling stock load spectrums is given in [41], however typical spacings are defined in Figure 12, where L_a is axle spacing, L_b is bogie spacing, and L_c is car spacing. The response of the track due to loading is affected by the static and dynamic stiffness of the guideway and soil. For example, if the support is soft, after one axle passes, the guideway may be still be in a suppressed downwards position by the time the subsequent axle arrives. This can then cause frequencies to be hidden by the bogie and car passage frequencies.

The superposition effect with respect to axle passage frequency is more clearly shown in Figure 13. For the homogenous ground, two axle passages are shown, spaced at 4.7m and moving at 50% and 100% of the critical velocity (note that 4.7m is larger than that for a typical train and is used as an example only). The dashed line shows the resulting time history due to superposition. It can be seen that there is an increase in the maximum magnitude of response, due to the individual axles influencing each other, however it is relatively minor. Constructive interference is only visible at the moments of time where the guideway is experiencing forced deflection due to the load.

In contrast, Figure 14 shows the same two axles with 4.7m spacing, however for layered ground 2, moving at both 50% and 100% of critical velocity. The 4.7m spacing corresponds to both the propagating wave vibration wavelength and the wavelength at the critical speed ($frequency = \frac{118m/s}{4.7m} = 25Hz$). At 50% of critical velocity constructive interference is minimal, however at 100% of critical velocity the response is altered significantly. For the faster speed, perturbations occur after the load passage corresponding to the propagating wave vibration wavelength. Then, because the vehicle axle spacing is also at the same wavelength, constructive interference occurs. Depending upon the ground properties, guideway properties, vehicle axle spacing and vehicle loads, the total response may be combination of constructive and/or destructive interference.
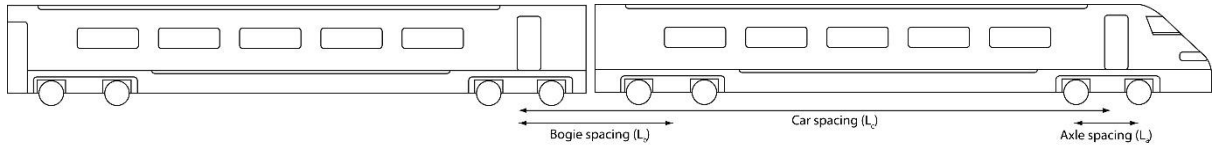
Figure 12 – Vehicle axle configuration
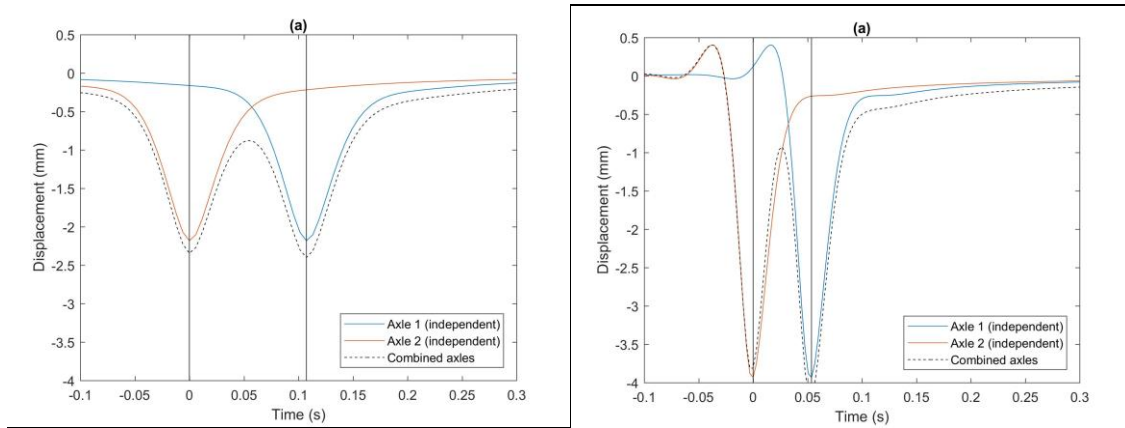
Figure 13 – Superposition of displacement response, a) Homogenous ground at V_{cv}=0.5, b) Homogenous ground at V_{cv}=1
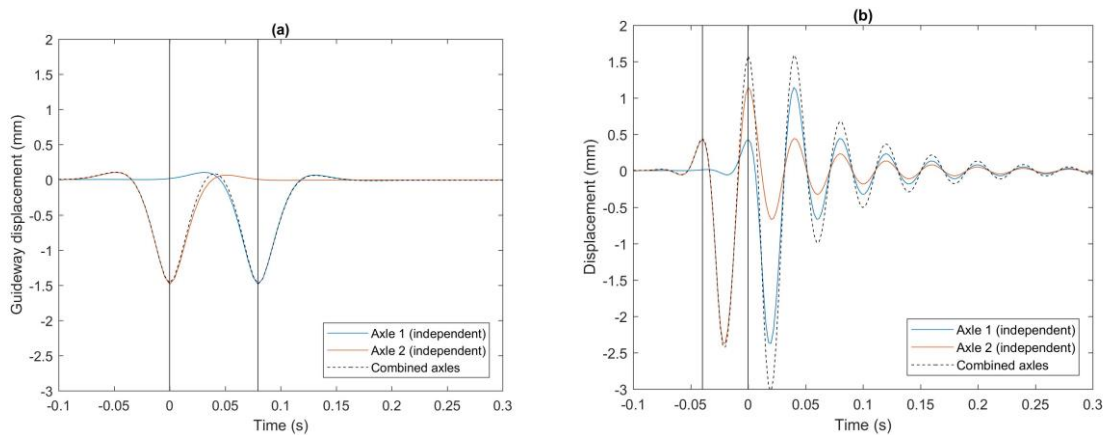
Figure 14 – Superposition of displacement response, a) Layered ground at V_{cv}=0.5, b) Layered ground at V_{cv}=1

Similar to the high speed train case, it is possible that future high speed vehicles will have axle-set configurations that give rise to multiple passage frequencies. However, for this study, to more concisely investigate the behaviour of axle spacings on guideway response, constant axle spacings are considered. Therefore Figure 15a shows the effect of multiple (10) axles instead of a single axle. For each train, axle spacing is assumed constant and is normalised as a function of guideway-ground propagating wave vibration wavelength. Note that some signals are truncated to remove unrealistically closely spaced axles as discussed previously. Also note that when the ratio of axle passing frequency to critical velocity frequency is low, it means axles are spaced far apart, and when it is high, it means the axles are spaced close together.

It is seen that at speeds below the critical velocity, the rail displacements remain almost constant regardless of axle spacing. Also when the axle spacing is large, for all speeds, the rail displacement values correspond to the values shown on the single axle <u>dynamic amplification curve (DAF - ~~DAF curve (~~</u>Figure 15b), indicating that the problem can be approximated as a series of independent loads. However, when the critical velocity is reached, only when the axle spacing is wide do the rail displacements correspond to the DAF curve values. Instead, as axle spacing decreases, and approaches the propagating wave vibration frequency of the guideway-ground-load system (shown in Figure 9b) large amplification occurs (i.e. when $V_{CV} \geq 1$). This amplification does not increase linearly with decreasing axle spacing though. Instead, this resonant condition occurs at different spacings for different ratios of critical velocity, because at high speeds, the resonant frequency changes with speed (Figure 9). In addition to the main peaks that occur when the axle-passage frequency is equal to F_{cv}, sub-peaks are also visible with increasing axle spacing. These are caused by two or more wavelengths occurring between adjacent wheels.

Figure 16a shows a similar figure to Figure 15a, however guideway uplift is instead plotted. Again, when there is a large distance between individual axles, the rail displacements in Figure 16a correspond to the single axle case (Figure 16b). Also, as recorded during field trials on high speed lines ([39]), uplift is more sensitive to increases in train speed compared to downward deflection. This is seen by comparing Figure 16b and Figure 15b, where the uplift at $V_{CV}=1$ is a much greater percentage of the static deflection value, when comparing the uplift to downward deflection.

Figure 17-Figure 18 also compare the deflections that occur solely due to critical velocity, versus those due to combined critical velocity and resonant effects. It is seen that at low speed, resonance has negligible effect, but starts to affect the response as the critical velocity is approached. At speeds greater than $V_{CV} \geq 0.8$, the resonant response starts to influence the results and at $V_{CV} \geq 1$ the resonant deflections dominate the magnitude of deflections. Therefore it is seen that when approaching the critical velocity, resonance can be much more important to consider compared to critical velocity alone. However, both effects are linked and resonance only occurs above critical velocity. Further, it should also be noted that if the total number of axles changes, displacement amplification may also change. Figure 15-Figure 17 are computed using 10 axles, however if different, the response may change (e.g. Figure 21).
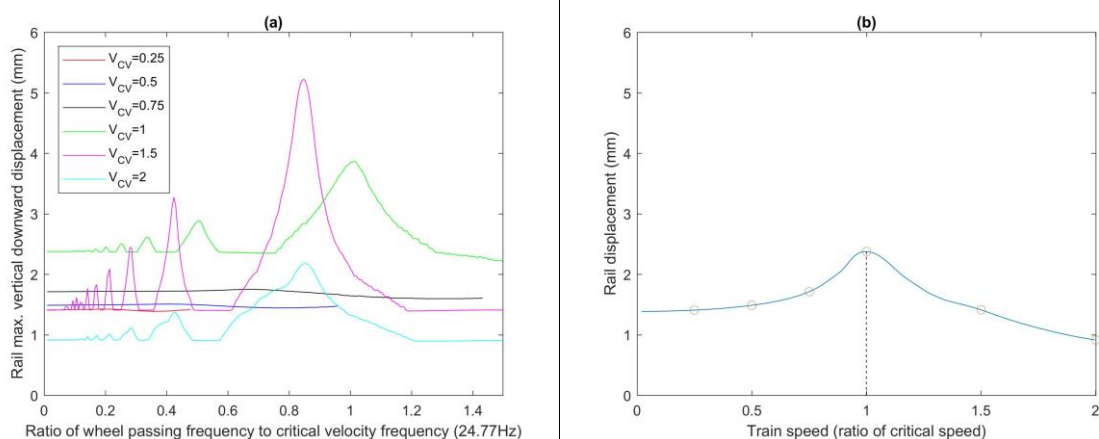
Figure 15 – The relationship between critical speed and axle spacing, a) downward displacement (note that smaller ratios indicate larger axle spacing), b) corresponding DAF curve (single axle)
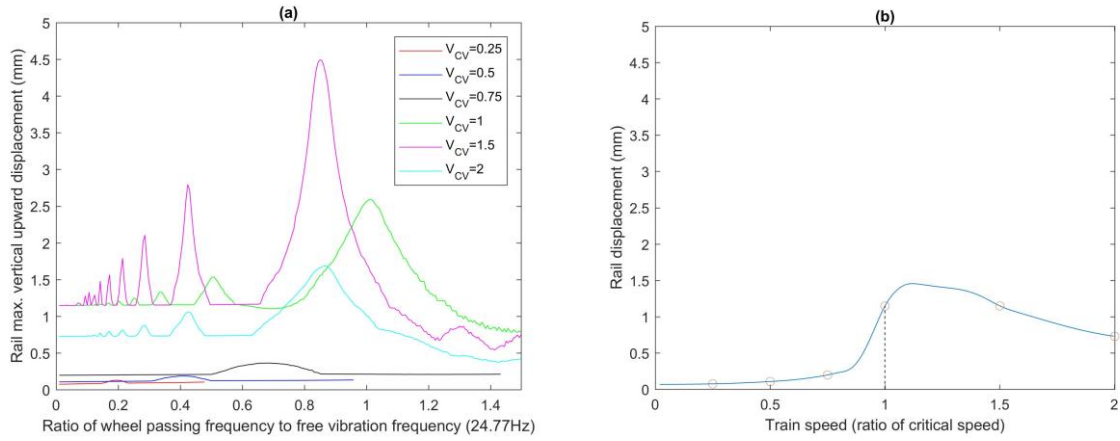
Figure 16 – The relationship between critical speed and axle spacing (note that smaller ratios indicate larger axle spacing), a) uplift displacement, b) corresponding DAF curve (single axle)
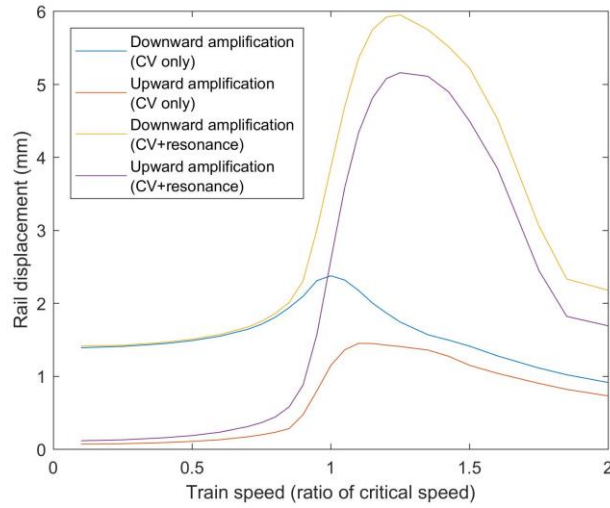
Figure 17 – The effect of critical speed on CV and resonance amplification considering all possible axle spacing combinations (soil 1 & guideway 2)
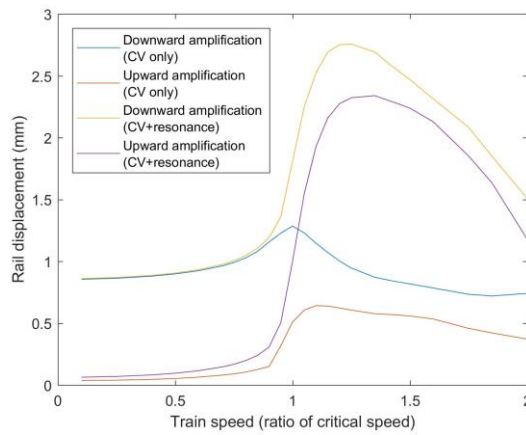
Figure 18 - The effect of critical speed on CV and resonance amplification considering all possible axle spacing combinations (soil 3 & guideway 2)

Figure 19 shows selected time histories corresponding to Figure 15a-Figure 16a, for V_{cv}=1 and V_{cv}=1.5. For plotting clarity purposes unitless time and truncating is used. To do so, the time response signals for each axle spacing are appended sequentially. Unitless time means that the timestep used for each of the three curves varies. For the 3 axle spacings chosen, displacements are largest when V_{cv}=1, and the effect of resonance is quite clear for all, with many instances of constructive and destructive superposition visible. For each case, propagating wave vibration is present after the 10 axles pass, however is more dominant at V_{cv}=1.5.
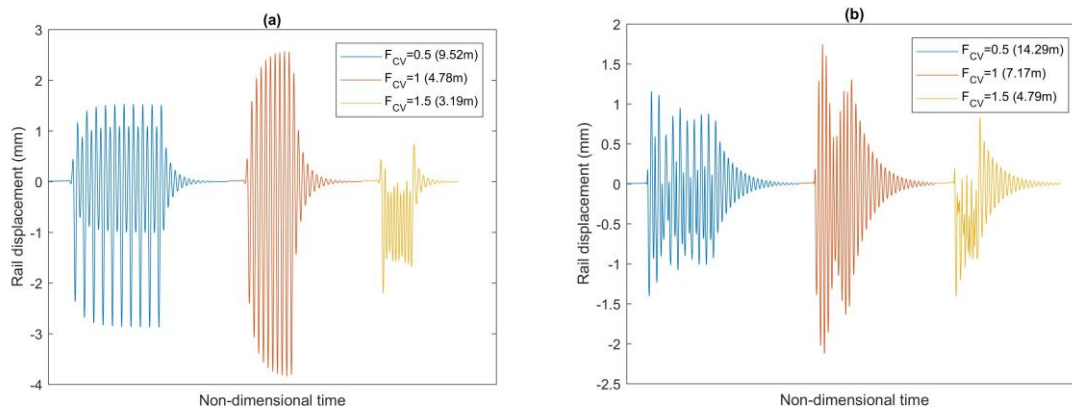
Figure 19 – Time histories of 10 axle train response with different spacings (soil 1 & guideway 2), a) V_{cv}=1, b) V_{cv}=1.5

4.2.1 Effect of the number of vehicle-guideway contact points

The previous section analysed the effect of 10 axles on displacement response. Depending upon vehicle type/configuration, this number may be significantly higher or lower. Therefore Figure 20 shows the effect of the number of axles on displacement response, when V_{cv}=1. The overall curve shape is similar to the 10-axle cases shown in figs Figure 15-Figure 16, with maximum amplification occurring at the critical velocity frequency, and lower magnitude peaks located at its sub-harmonics. This is because the guideway and ground structures are constant regardless of the number of axles, and therefore the propagating wave vibration frequency doesn't change.

To analyse the effect of axle spacing in more detail though, Figure 21 shows the effect of axle count on maximum rail displacement, when V_{cv}=1 and V_{cv}=1.5. The displacements are normalised to the maximum 2-axle displacement, rather than 1-axle which is typically used to compute dynamic amplification curves. It is seen that for both cases, when the total number of axles is low, displacements are highly sensitive to changes in axle number. However as the number of total axles increases, sensitivity decreases, which is consistent with Figure 20. This is true for all guideway and soil combinations. It is noticeable though that the relationship between displacements and total axles is different when comparing V_{cv}=1 and V_{cv}=1.5. At the higher speed, displacements are still increasing slightly when 32 axles are present, while at lower speed the displacements are largely constant in the same axle range. This increase in displacements is due to additional superposition and the guideway not fully recovering to its neutral position before the next axle has arrived.

This finding is important because many vehicles are formed from a finite number of discrete cars/carriages. Therefore in reality there are likely to be several distinct axle spacings associated with the vehicle configuration (e.g. axle, bogie and car spacings), which correspond to a variety of sub-harmonics in the frequency domain. Then, considering amplification can be induced by the spacing between only 2 axles, resonant amplification may become more problematic than entirely

uniform spaced axles. For example, Figure 20 shows numerous distinct and localised peaks depending upon the relationship between axle passing frequency and propagating wave vibration frequency. If there are multiple dominant axle passing frequencies, then these peaks have the potential to merge and rail deflection will undergo complex amplification compared to the single axle case.
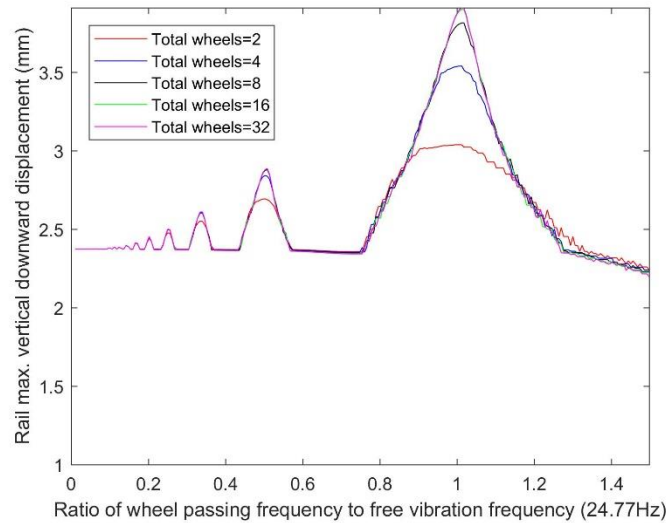
Figure 20 – The effect of total number of axles and their spacing on rail displacement (soil 1, guideway 2 & V_{CV}=1.0)
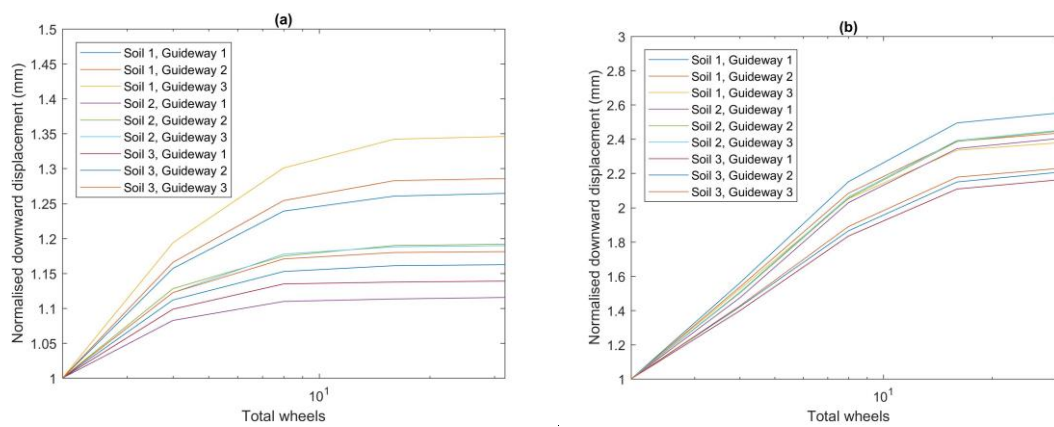
Figure 21 – The effect of total number of axles on normalised rail displacement, a) V_{CV}=1, b) V_{CV}=1.5. Note that horizontal axis is log-scale ranging from 1-32 wheels

5. Discussion

The current railway speed record is 603km/h, while the aspirational maximum speeds of vacuum transport (e.g. hyperloop) and car technology (e.g. Bloodhound SSC) are 1200 km/h and 1600 km/h respectively. Further, the engineered Young's modulus of earthwork structures that support transport infrastructure are often in the region of 100-250MPa, which is equates to shear

wave velocities in the range 360-900km/h. Therefore, depending upon guideway stiffness, future transport systems may need to operate, at least in-part, in the range 1<V_{CV}<2.

This is problematic because guideway-ground resonance occurs in the presence of multiple moving loads at speeds close to, and above, the critical velocity. When considering Figure 17, it is seen that resonance results in very large dynamic amplifications in the range 1< V_{CV}<2 (i.e. the speed range of future aspirational transport systems). This is due to coincidence between the frequency of axle spacing and the guideway-ground propagating wave vibration frequency, and yields much greater amplification than simply the 'critical velocity effect' commonly considered on high speed rail lines. Therefore axle spacing is an increasingly important consideration when designing transport systems operating at V_{CV}≥1. This will require more multi-disciplinary design approaches compared to existing industries where vehicles and guideway sub-structures are typically designed independently.

Therefore, assuming V_{CV}≈1 is the speed at which the axle spacing becomes important, the axle spacing that will give significant amplification at this speed is:

$$axle\ spacing = \frac{\cancel{V_{cv}}Crticial\ velocity}{\cancel{F_{cv}}Critical\ velocity\ frequency}$$

Considering the relatively minor change in guideway-ground resonant frequency for CV≥1 (Figure 10), a scoping assessment can be performed by only checking all axle spacings greater than this value during design. As an example, considering the soil 2-guideway 1 case discussed previously, the critical axle spacing is 3.75m, which is close to the typical bogie/axle spacing on high speed trains (axle spacing is typically 2.5-3m). Therefore there is a risk of resonant effects occurring when close to critical velocity.

It is also shown that displacement amplification increases with the total number of axles, with even just 2 axles inducing amplification (i.e. meaning it is relevant for future car technologies such as Bloodhound SSC). When the number of axles exceeds a critical threshold, adding further axles results in minimal additional amplification. Considering amplification occurs for just 2 axles, it is likely that unevenly spaced axles will generate a larger number of amplification peaks at each speed. Due to superposition these peaks may possibly result in similar or lower amplification, depending upon train speed. Further, in reality, vehicles are configured in groups of axles with regular, but varied spacing. This will increase the complexity of interference.

Finally, it should be noted that the analysis in this paper is based upon a high speed rail inspired guideway. This is in-part because vacuum transport infrastructure technology is still in its infancy, without a universal design for either vehicles or guideway/infrastructure. However, it should be noted that Hyperloop tube sections are likely to have a higher bending stiffness compared to the track studied here. Further analysis is required to assess the effect of magnet/axle spacing and resonance for bespoke infrastructure/vehicle arrangements. Also, this analysis assumes the soil only experiences low strain and behaves in a linear elastic manner. In reality, if high displacements occur due to resonant effects, displacement amplitudes may be further magnified due to soil stiffness degradation, which is also highly sensitive to axle spacing.

6. Conclusions

The operational speed of ground transport systems is growing rapidly. Proposed speeds indicate that vehicles may operate, at least on some sections of their network, between 100-200% of the

guideway-ground critical velocity. It is known that as moving load speeds approach the critical velocity of their support system, large dynamic effects are generated that result in high displacements. However, the effect of axle/magnet spacing on dynamic amplification is still unclear. Therefore, for the first time, this paper analyses the effect of multiple loads moving at speeds above the critical velocity. First a numerical model is developed and then validated using field data. It is used to show:

1. When vehicles operate at speeds greater than the critical velocity, vehicle axle spacing plays a dominant role in the displacement amplification of the guideway system
2. Maximum guideway amplification occurs when the vehicle axle frequency is equal to the propagating wave vibration frequency of the guideway-ground system.
3. At speeds lower than the critical velocity the guideway-ground system does not vibrate freely, meaning it cannot experience amplification due to resonance. At speeds below this, displacements are relatively constant regardless of axle spacing, unless axles are configured very close together
4. Resonance can have a greater effect on displacement magnification compared to critical velocity effects. For the case study shown, although critical velocity might increase displacements by 50-100%, for the same scenario, resonance can increase displacements by 400%
5. Resonant amplification can occur in the presence of 2+ axles, thus making it relevant to all practical high speed vehicle types with discrete axle/magnet spacings. If a vehicle has a large number of regularly spaced axles, dynamic response will be magnified at the corresponding wavelengths. Alternatively, if a vehicle has a large number of irregularly spaced axles, a broader range of wavelengths will be subject to amplification.

Acknowledgments

References

1   Musk E. *Hyperloop Alpha white paper*. ; 2013.

2   Evans B, Rose C. Simulating the aerodynamic characteristics of the Land Speed Record vehicle BLOODHOUND SSC. *Proc Inst Mech Eng Part D J Automob Eng* 2014; **228**:1127–1141.

3   Alexander NA, Kashani MM. Exploring Bridge Dynamics for Ultra-high-speed, Hyperloop, Trains. *Structures* 2018; **14**:69–74.

4   Ruiz JF, Soares PJ, Costa PA, Connolly DP. The effect of tunnel construction on future underground railway vibrations. *Soil Dyn Earthq Eng* 2019; **125**:105756.

5   Olivier B, Connolly DP, Alves Costa P, Kouroussis G. The effect of embankment on high speed rail ground vibrations. *Int J Rail Transp* 2016; **4**:229–246.

6   Kouroussis G, Connolly DP, Olivier B, Laghrouche O, Alves Costa P. Railway cuttings and embankments: Experimental and numerical studies of ground vibration. *Sci Total Environ* 2016; **557–558**:110–122.

7   Woldringh RF, New BM. Embankment design for high speed trains on soft soils. In: *Proceedings of the 12th European Conference on Soil Mechanics and Geotechnical Engineering*.Amsterdam, Netherlands: ; 1999. pp. 1703–1712.

8   Huang H, Chrismer S. Discrete element modeling of ballast settlement under trains moving at "Critical Speeds." *Constr Build Mater* 2013; **38**:994–1000.

9   Krylov V, editor. *Ground Vibrations From High-Speed Railways: Prediction And Mitigation*. ICE Publishing; 2019.

10   Yu Z, Woodward PK, Laghrouche O, Connolly DP. True triaxial testing of geogrid for high speed railways. *Transp Geotech* 2019; **20**. doi:10.1016/j.trgeo.2019.100247

11   Dong K, Connolly DP, Laghrouche O, Woodward PK, Alves Costa P. The stiffening of soft soils on railway lines. *Transp Geotech* Published Online First: 2018. doi:10.1016/j.trgeo.2018.09.004

12   Lamb H. On the propagation of tremors over the surface of an elastic solid. *Philos Trans R Soc London Ser A, Contain Pap a Math or Phys Character* 1904; **203**:1–42.

13   Kenney J. Steady-state vibrations of beam on elastic foundation for moving load. *J Appl Mech* 1954; **76**:359–364.

14   Fryba L. *Vibration of Solids and Structures Under Moving Loads*. Groningen, The Netherlands: Noordhoff International Publishing; 1972.

15   Krylov V. Generation of ground vibrations by superfast trains. *Appl Acoust* 1995; **44**:149–164.

16   Dieterman H, Metrikine A. The Equivalent stiffness of a half-space interacting with a beam. Critical velocities of a moving load along the beam. *Eur J Mech - A/Solids* 1996; **15**:67–90.

17   Barros F, Luco JE. Stresses and displacements in a layered half-space for a moving line load. *Appl Math Comput* 1995; **67**:103–134.

18   Sheng X, Jones CJC, Thompson DJ. A comparison of a theoretical model for quasi-statically and dynamically induced environmental vibration from trains with measurements. *J Sound Vib* 2003; **267**:621–635.

19   Ferrara R, Leonardi G, Jourdan F. A Two-Dimensional Numerical Model to Analyze the Critical Velocity of High Speed Infrastructure The 2D Numerical Model. In: *Proceedings of the fourteenth international conference on civil, structural and environmental engineering computing*.; 2013. pp. 1–16.

20   Yang LA, Powrie W, Priest JA. Dynamic Stress Analysis of a Ballasted Railway Track Bed during Train Passage. *J Geotech Geoenvironmental Eng* 2009; **135**:680.

21   Nsabimana E, Jung Y-H. Dynamic subsoil responses of a stiff concrete slab track subjected to various train speeds: A critical velocity perspective. *Comput Geotech* 2015; **69**:7–21.

22   Connolly D, Giannopoulos A, Fan W, Woodward PK, Forde MC. Optimising low acoustic impedance back-fill material wave barrier dimensions to shield structures from ground borne high speed rail vibrations. *Constr Build Mater* 2013; **44**:557–564.

23   Varandas JN, Hölscher P, Silva MAG. Dynamic behaviour of railway tracks on transitions zones. *Comput Struct* 2011; **89**:1468–1479.

24   Galvin P, Domínguez J. Analysis of ground motion due to moving surface loads induced by high-speed trains. *Eng Anal Bound Elem* 2007; **31**:931–941.

25   Kouroussis G, Verlinden O, Conti C. Free field vibrations caused by high-speed lines: Measurement and time domain simulation. *Soil Dyn Earthq Eng* 2011; **31**:692–707.

26   Hall L. Simulations and analyses of train-induced ground vibrations in finite element models.

Soil Dyn Earthq Eng 2003; **23**:403–413.

27   Kouroussis G, Connolly DP, Vogiatzis K, Verlinden O. Modelling the environmental effects of railway vibrations from different types of rolling stock - A numerical study. *Shock Vib* 2015; :1–15.

28   Shih JY, Thompson DJ, Zervos A. The effect of boundary conditions, model size and damping models in the finite element modelling of a moving load on a track/ground system. *Soil Dyn Earthq Eng* 2016; **89**:12–27.

29   Galvin P, Romero A, Domínguez J. Fully three-dimensional analysis of high-speed train–track–soil-structure dynamic interaction. *J Sound Vib* 2010; **329**:5147–5163.

30   Andersen L, Nielsen SRK, Krenk S. Numerical methods for analysis of structure and ground vibration from moving loads. *Comput Struct* 2007; **85**:43–58.

31   Colaço A, Alves Costa P, Connolly DP. The influence of train properties on railway ground vibrations. *Struct Infrastruct Eng* 2016; **12**:517–534.

32   Alves Costa P, Calçada R, Silva Cardoso a. Track–ground vibrations induced by railway traffic: In-situ measurements and validation of a 2.5D FEM-BEM model. *Soil Dyn Earthq Eng* 2012; **32**:111–128.

33   Alves Costa P, Calcada R, Cardoso AS, Bodare A. Influence of soil non-linearity on the dynamic response of high-speed railway tracks. *Soil Dyn Earthq Eng* 2010; **30**:221–235.

34   Woodward PK, Laghrouche O, Mezher SB, Connolly DP. Application of coupled train-track modelling of critical speeds for high-speed trains using three-dimensional non-linear finite elements. *Int J Railw Technol* 2015; **4**:1–35.

35   Dong K, Connolly DP, Laghrouche O, Woodward PK, Alves Costa P. Non-linear Soil Behaviour on High Speed Rail Lines. *Comput Geotech* 2019; **112**:302–318.

36   Alves Costa P. *Vibrações Do Sistema Via-Maciço Induzidas Por Tráfego Ferroviário . Modelação Numérica E Validação Experimental (PhD thesis)*. 2011.

37   Mezher SB, Connolly DP, Woodward PK, Laghrouche O, Pombo J, Costa PA. Railway critical velocity - Analytical prediction and analysis. *Transp Geotech* 2016; **6**:84–96.

38   Steenbergen MJMM, Metrikine A V. The effect of the interface conditions on the dynamic response of a beam on a half-space to a moving load. *Eur J Mech A/Solids* 2007; **26**:33–54.

39   Madshus C, Kaynia AM. High-Speed Railway Lines on Soft Ground: Dynamic Behaviour At Critical Train Speed. *J Sound Vib* 2000; **231**:689–701.

40   Kramer S. *Geotechnical Earthquake Engineering*. Prentice Hall; 1996.

41   Milne DRM, Le Pen LM, Thompson DJ, Powrie W. Properties of train load frequencies and their applications. *J Sound Vib* 2017; **397**:123–140.